

## *Supporting Information*

### Experimental and Mechanistic Study of Stabilized Dry CO<sub>2</sub> Foam Using Polyelectrolyte Complex Nanoparticles Compatible with Produced Water to Improve Hydraulic Fracturing Performance

<sup>1</sup>Hooman Hosseini, <sup>2</sup>Jyun Syung Tsau, <sup>2</sup>Karen Shafer-Peltier, <sup>3,4</sup>Craig Marshall, <sup>5</sup>Qiang Ye, <sup>1</sup>Reza Barati  
Ghahfarokhi\*

<sup>1</sup>Department of Chemical and Petroleum Engineering, University of Kansas, Lawrence, Kansas  
66045, USA

<sup>2</sup>Tertiary Oil Recovery Program, University of Kansas, Lawrence, Kansas 66045, USA

<sup>3</sup>Department of Geology, University of Kansas, Lawrence, Kansas 66045, USA

<sup>4</sup>Department of Chemistry, University of Kansas, Lawrence, Kansas 66045, USA

<sup>5</sup>Institute for Bioengineering Research, University of Kansas, Lawrence, Kansas 66045, USA

Correspondence to: R. Barati (E-mail: [rezab@ku.edu](mailto:rezab@ku.edu))

### Surfactant specification:

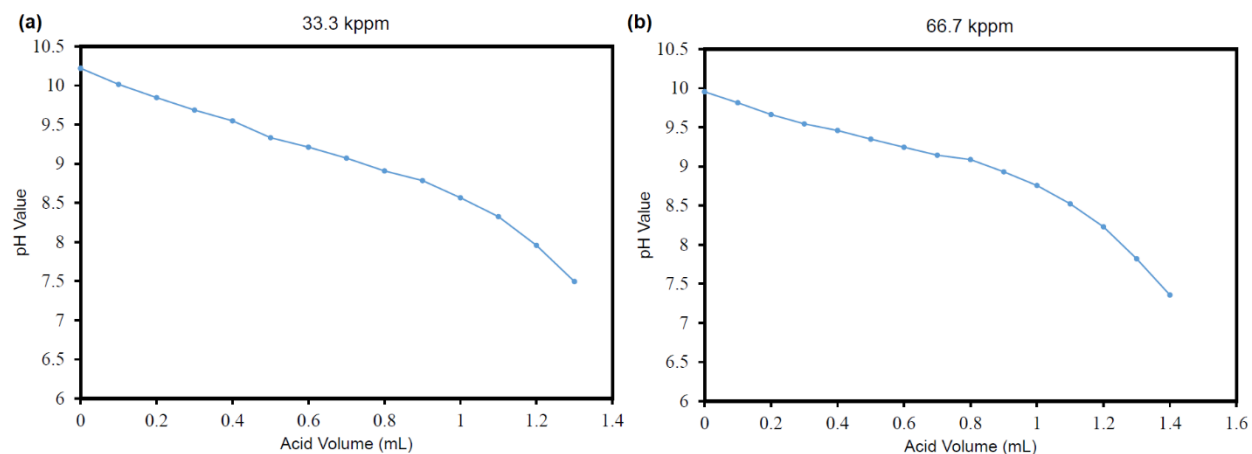
The main ingredients in the form of solvent and additive to the surfactant solutions are listed in Table S1.

Table S1. Solvent and additives in HDP-0761-12-2AM surfactant provided by Harcros

Chemical Name	CAS number	%
Water	7732-18-5	60 -< 70
Sodium Chloride	7647-14-5	5 -< 10
3-chloro-1,2-Propanediol	96-24-2	< 0.2
Other components below reportable levels	-	30 -< 40

### Titration curves for pH adjustments:

pH calibration curves for HCL 6N amount added to PEI 1 wt% solution in 33.3 kppm and 66.7 kppm are shown in Figure S1.



**Figure S1.** pH calibration curves for HCL 6N amount added to PEI 1 wt% solution in 33.3 kppm and 66.7 kppm brine solutions

### **Fourier Transform Infrared spectroscopy:**

The zwitterionic surfactant was characterized with Fourier transform-Infrared spectroscopy (FT-IR) to identify the chemical functional groups. As Figure S2 illustrates there exist characteristic bands for the surfactant mixture between 970 to 1575  $\text{cm}^{-1}$  as well as between 2800 to 3000  $\text{cm}^{-1}$ , which were not present in water spectrum (blue curve). As the majority of surfactant is composed of water (60-70 w/w % per Table 2), water bands (1580 to 1680  $\text{cm}^{-1}$ , 2000 to 2220  $\text{cm}^{-1}$  and 3000 to 3700  $\text{cm}^{-1}$ ) dominate the surfactant spectrum.

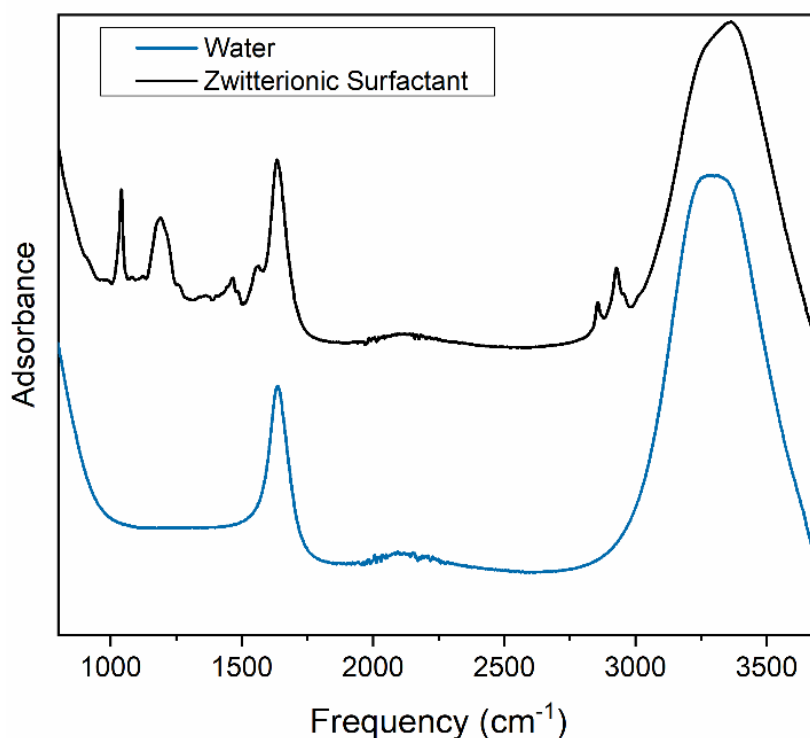


**Figure S2.** Fourier transform infrared spectra for water and Zwitterionic surfactant used in this study

Stretching vibrations for alkyl aryl ether (C-O) and sulfonate and sulfonamide (S=O) chemical bonds were observed at 1177  $\text{cm}^{-1}$ . Medium bending for methyl group (C-H) was identified at 1457  $\text{cm}^{-1}$  followed by medium to weak bending located at 1570  $\text{cm}^{-1}$  for the amine

group (N-H). Presence of other bending for amine, strong stretches for alkene, secondary amine and ketone are anticipated, however, coverage by H-O-H scissors in water overwhelmed the aforementioned bands. Medium adsorptions at 2850 and 2924  $\text{cm}^{-1}$  belong to C-H stretch in alkane and aldehyde (doublet). The down field bands such as expected surfactant amine stretches (N-H) and hydroxide (O-H) in the range of 3000 to 3700  $\text{cm}^{-1}$  were covered by strong stretch resulted from the O-H bond from water molecules. The main functional groups are quaternary and secondary amines as well as pendant hydroxide groups, amide and sulfonate ( $\text{R-SO}_3^-$ ). Combination of ammonium and sulfonate offers a zwitterionic surfactant with both cationic and anionic charge head groups capable of conjunction with PECNP in  $\text{scCO}_2$  lamella interface.

### Air-foam stability setup:

Figure S3 illustrates the setup for air-foam stability measurements.

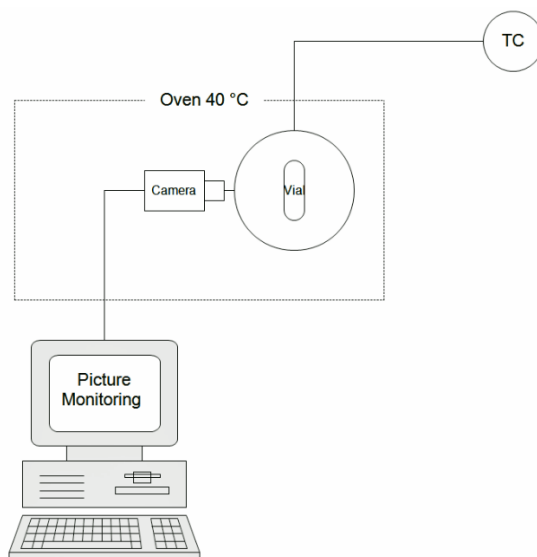


**Figure S3.** Simple vial test for PECNP/Surfactant mixtures in high salinity brine mixed with air as preliminary test before actual test with  $\text{scCO}_2$ . Reprinted with permission from [1] Copyright SPE 2018.

### **Elasticity calculations:**

Dilatational elasticity was estimated according to ramp-type perturbation approach previously presented by Boury and coworkers [2]. To describe the surface pressure change during the time T, sum of equilibrium and non-equilibrium portions are considered as following:

$$(1) \quad \Delta\pi = \Delta\pi_e + \Delta\pi_{ne}$$

The variation of interfacial pressure after compression of equilibrated surface layer of pendant drop is correlated to surface area variation as a result of mechanical strain to estimate the equilibrium surface dilatational elasticity as it is depicted in figure S4-a,b [2,3]:

$$(2) \quad \Delta\pi_e = E_e \frac{U_b t}{A_i}$$

Where  $A_i$  surface area prior to applying the mechanical strain and this equivalency is introduced:

$$(3) \quad \frac{U_b t}{A_i} = \frac{\Delta A}{A_i}$$

The elastic model for strain analysis of lamella after inducing the perturbations is represented in Figure S4-c.

The non-equilibrium portion is also calculated based upon dissipation of accumulated energy during compression and relaxation as it is depicted in figure S4-d [2].

$$(4) \quad \Delta\pi_{ne} = \frac{E_{ne} U_b t}{A_i} \left(1 - e^{-\frac{t}{\tau}}\right)$$

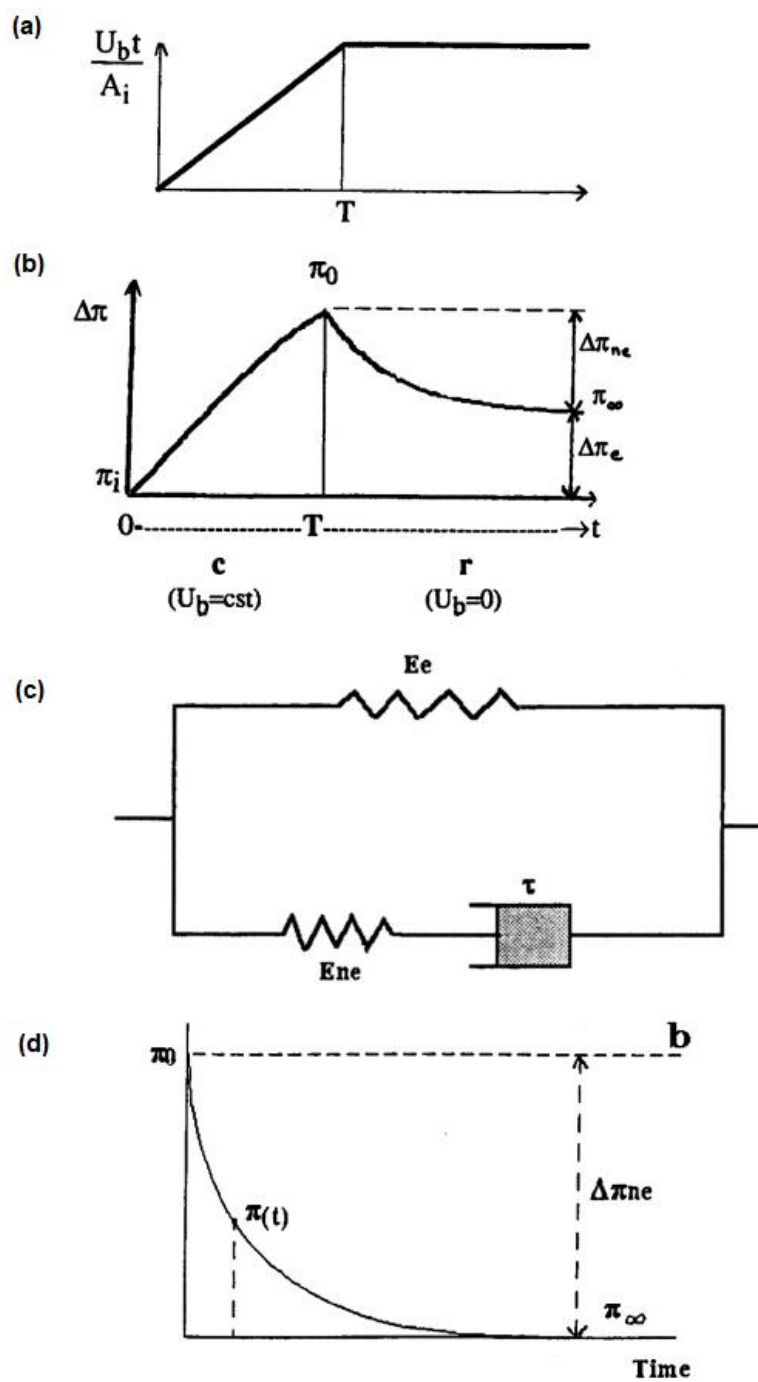


**Figure S4.** Rheological model of the monolayer representing the mechanical strain and surface pressure change with time  $T$  and two different portions of elasticity in form of equilibrium and non-equilibrium. Reprinted with permission from [3] Copyright 1995 ACS.

Examples of calculations for ionic mixtures in 33.3 kppm and 66.7 kppm high salinity

brine are shown in Table S2 and S3.

**Table S2.** Summary of elasticity calculations from interfacial tension analysis in 33.3 kppm systems

System	Initial $\pi$	Final $\pi$	$\Delta\pi(\text{ne})$	$\Delta\pi(\text{e})$	Initial A	Final A	$\Delta A$	$\Delta A/A_i$	Ee
RO-Water-scCO <sub>2</sub>	32.21	24.91	7.3	24.91	18.87	14	4.87	0.26	96.52
33.3kppm-scCO <sub>2</sub>	31.51	28.7	2.81	28.7	18.86	20.04	1.18	0.066	458.71
33.3kppm-Surf-scCO <sub>2</sub>	5.95	5.59	0.36	5.59	7.41	3.79	3.62	0.49	11.44
33.3kppm-PECNP:Surf 1:9 scCO <sub>2</sub>	6.27	5.76	0.51	5.76	5.25	4.39	0.86	0.16	35.16

**Table S3.** Summary of elasticity calculations from interfacial tension analysis in 66.7 kppm systems

System	Initial $\pi$	Final $\pi$	$\Delta\pi(\text{ne})$	$\Delta\pi(\text{e})$	Initial A	Final A	$\Delta A$	$\Delta A/A_i$	Ee
RO-Water-scCO <sub>2</sub>	32.21	24.91	7.3	24.91	18.87	14	4.87	0.26	96.52
66.7kppm-scCO <sub>2</sub>	29.93	27.14	2.79	27.14	20.9	21.9	1	0.05	567.23
66.7kppm-Surf-scCO <sub>2</sub>	5.64	7.39	1.75	7.39	4.7	5.94	1.24	0.265	28.01
66.7kppm-PECNP:Surf 4:6 scCO <sub>2</sub>	6.78	6.34	0.44	6.34	4.96	5.3	0.34	0.07	92.49

### Air-foam stability test results:

For initial stage of stability measurements the foaming mixture was mixed with air as shown in Figure S5. The foam height was measured with respect to time.

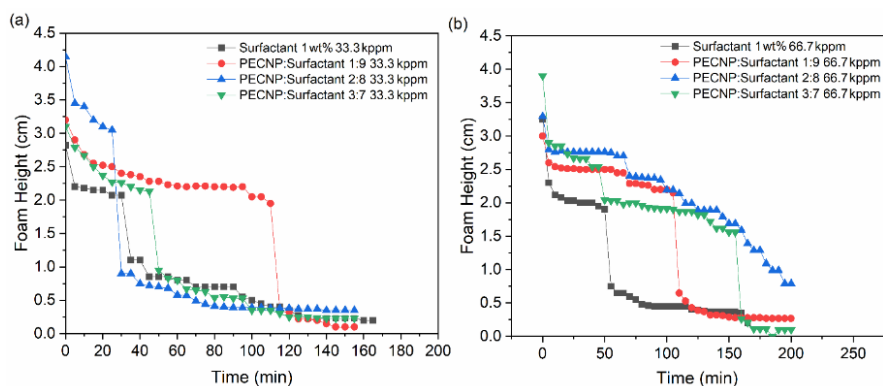


**Figure S5.** Preliminary foam stability test for different ratios of PECNP to Surfactant mixed with air for two different brine concentrations (a) 33.3 kppm and (b) 66.7 kppm. Reprinted with permission from [1] Copyright SPE

### **Rheological measurements:**

The rheometer setup consists of feed cylinders, pumps, the main rheometer unit connected to a PC software and a waste pump collector. To maintain isothermal conditions in lines, valves and pumps, a recirculating cooler (ISOTEMP 1016D) and heating tapes were used and the temperature was set to 6°C. Pump A is refilled with CO<sub>2</sub> and temperature and pressure were set to a supercritical state of 40°C and 1350 psi. Pump B was also filled with the foaming liquid. Lines containing scCO<sub>2</sub> and foaming solution were connected and the produced foam flowed through the rheometer cup and from there to the waste collector pump (Pump C). The proportion of scCO<sub>2</sub> to foaming mixture was chosen to be 9 to 1 based on previous observations by our group [4,5]. Rheometer utilizes constant (2000 s<sup>-1</sup>) and variable (2000 s<sup>-1</sup> to 100 s<sup>-1</sup>) shear rates. The measurements were carried out in dynamic (constant flow of foam solution), static (stagnant foam liquid in the cup) and ramp (variable shear rate in static mode). During the static and ramp modes 45 to 120 data points were collected with 30-second time intervals. The Rheoplus software was used to set the rheological adjustments. The main rheometer unit was connected to a PC software and a waste pump collector.

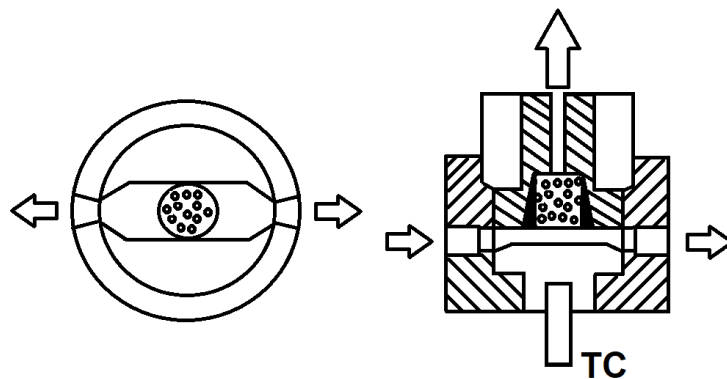
The flow consistency index depicts the highest value for optimal concentrations of PECNP and WLMs shown in Table S4.

Table S4. Flow consistency index (K) and flow behavior index (n) for variety of PECNP/Surfactant scCO<sub>2</sub> foam systems. Reprinted with permission from [1] Copyright SPE 2018.

33.3 kppm System		K (Pa s <sup>n</sup> )	n
Surfactant-scCO <sub>2</sub>		1184.3	0.402
PECNP:Surfactant-scCO <sub>2</sub> (3:7)		1387.9	0.394
PECNP:Surfactant-scCO <sub>2</sub> (2:8)		1261.6	0.407
PECNP:Surfactant-scCO <sub>2</sub> (1:9)		2916.4	0.276
66.7 kppm System		K (Pa s <sup>n</sup> )	n
Surfactant-scCO <sub>2</sub>		1035.7	0.368
PECNP:Surfactant-scCO <sub>2</sub> (4:6)		1683.1	0.380
PECNP:Surfactant-scCO <sub>2</sub> (3:7)		1443	0.371
PECNP:Surfactant-scCO <sub>2</sub> (2:8)		1163.9	0.405
PECNP:Surfactant-scCO <sub>2</sub> (1:9)		1464.6	0.385

**Fluid loss:**

The fluid loss module is presented in Figure S6 as a core sits adjacent to the fluid flow path and degree of fracturing fluid flow and leak-off in low permeability rocks were measured. The scCO<sub>2</sub> foam was generated and directed to the fluid loss setup where the tight core was exposed to foam flow. Two pathways directed the flow through the cell, one was adjacent to the core and the other through the core (fluid loss). The volume of gas and liquid coming out of the core were recorded versus time.



**Figure S6.** Fluid loss module from different views used in HPHT CO<sub>2</sub> foam apparatus (side and top view).

Reprinted with permission from [1] Copyright SPE 2018.

The volume loss (gas and liquid) belong to the surfactant and PECNP:Surfactant systems penetrated through the Kentucky limestone core placed in the module (figure S6) is shown in figure S7.

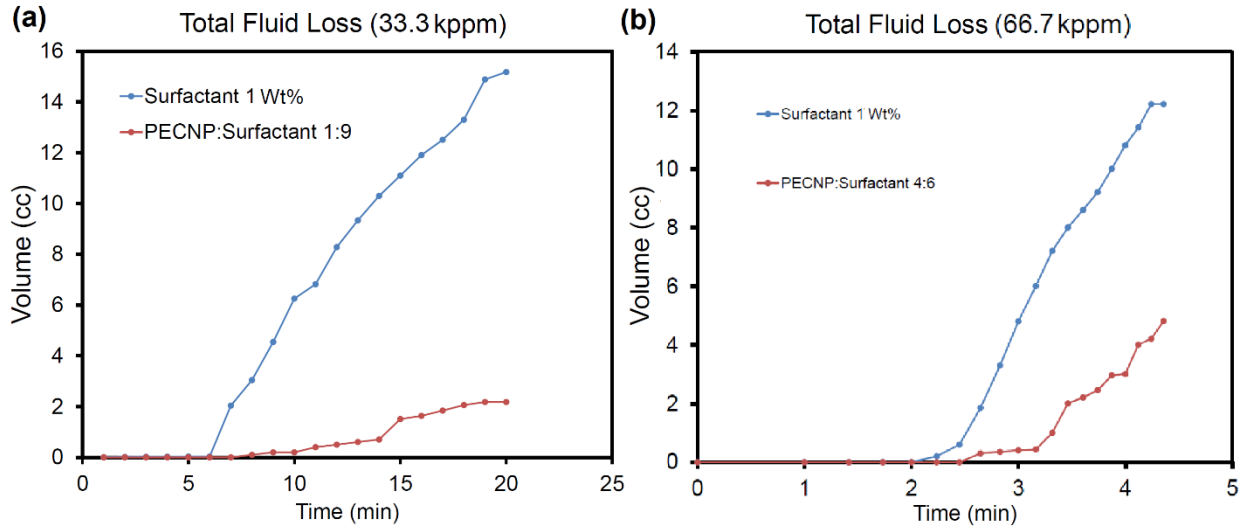


**Figure S7.** Volume of gas and liquid fluid loss for surfactant and PECNP:Surfactant mixtures in (a) 33.3kppm and (b) 66.7kppm high salinity brine

The Permeability of the core before and after the foam flood through the module was measured (Table S5) and the results indicated no significant change in the permeability of tight cores (varying between 0.18 to 0.23 mD). Here is the example of permeability measured before and after fluid loss experiment with surfactant 1 wt% and PECNP:Surf 4:6 in 66.7 kppm brine. The permeability was calculated for each individual core sample according to Darcy's law with the flow rate of 0.1, 0.3 and 1 mL/min.

**Table S5.** Summary of permeability calculations from core flood analysis on Kentucky Sandstone tight core in 66.7kppm systems

Core	Fluid Loss Liquid	Slope	KA/ $\mu$ L	$\mu$ (cP)	A (cm <sup>2</sup> )	L (cm)	K (D)	K(mD)
Kentucky	-	0.0005	0.0005	1.05	5.08	2.23	0.000231	0.23
Kentucky	Surf 1% 66.7kppm	0.0005	0.0005	1.05	5.08	2.23	0.000231	0.23
Kentucky	PECNP:Surf 4:6 66.7 kppm	0.0004	0.0004	1.05	5.08	2.23	0.000185	0.18

### Sand pack test:

The sand pack experiment included a primary brine flood to measure the initial pack permeability, an oil flood for complete saturation, a foam flood for clean-up and a secondary brine flood for secondary packed bed permeability. The flood scenarios and apparent viscosities for different scenarios of flood in the sandpack is represented in Table S6.

**Table S6.** Flood scenarios and mobility features for surfactant, oil and scCO<sub>2</sub> foam floods in the sand pack

Sand pack scenarios	PV (cm <sup>3</sup> )	Q (cm <sup>3</sup> /s)	k (D)	ΔP (psi)	μ <sub>app</sub> (cP)
33.3 kppm Brine Flood	7.58	0.1	169.94	0.38	0.93
Oil Flood	7.58	0.1	169.94	2.71	6.66
Surf 1 wt% scCO <sub>2</sub> Flood	7.58	0.1	169.94	6.00	14.75
Secondary Brine Flood	7.58	0.1	154.22	0.32	0.71
33.3 kppm Brine Flood	7.63	0.1	154.23	0.48	1.07
Oil Flood	7.63	0.1	154.23	2.42	5.4
PECNP:Surf 1:9 scCO <sub>2</sub> Flood	7.63	0.1	154.23	8.43	18.8
Secondary Brine Flood	7.63	0.1	157.77	0.35	0.8
66.7 kppm Brine Flood	7.41	0.1	155.14	0.56	1.26
Oil Flood	7.41	0.1	155.14	2.87	6.44
Surf 1 wt% scCO <sub>2</sub> Flood	7.41	0.1	155.14	4.02	9.02
Secondary Brine Flood	7.41	0.1	156.12	0.34	0.77
66.7 kppm Brine Flood	7.47	0.1	154.91	0.43	0.96
Oil Flood	7.47	0.1	154.91	2.66	5.96
PECNP:Surf 4:6 scCO <sub>2</sub> Flood	7.47	0.1	154.91	5.56	12.46
Secondary Brine Flood	7.47	0.1	143.87	0.36	0.75

The pressure drop profile for each condition is presented in Figure S8 to S11 for the cases where the 33.3 kppm brine is used.

## Primary brine flood

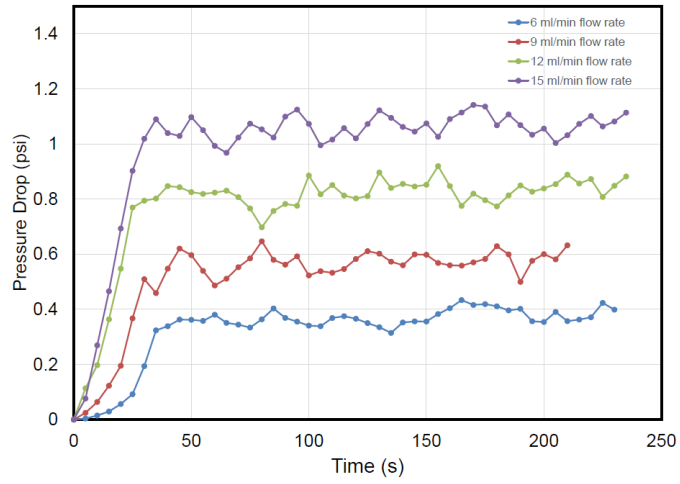


**Figure S8.** Primary brine flood in the proppant filled packed bed with 33.3 kppm high salinity brine

## Oil flood

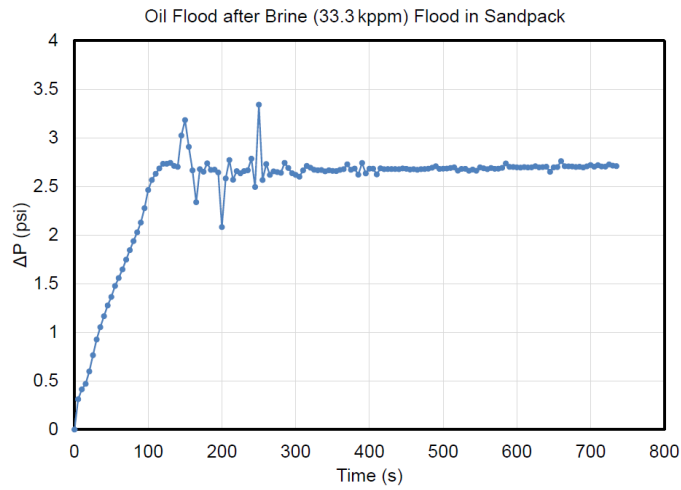


**Figure S9.** Oil Flood in the proppant filled packed bed saturated with 33.3 kppm high salinity brine

## Foam flood

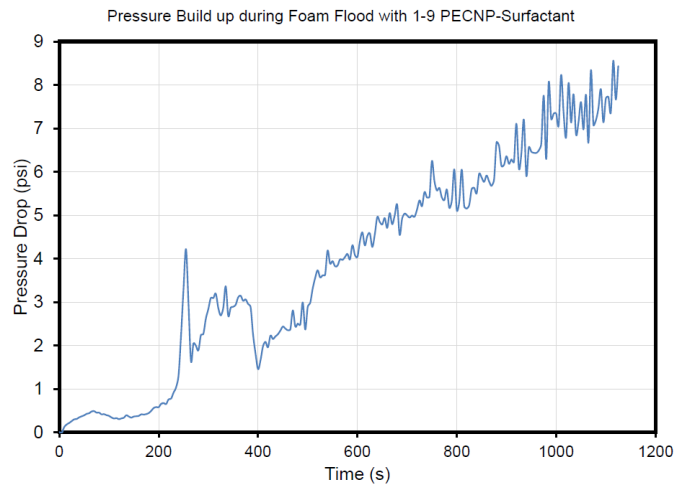


**Figure S10.** Foam Flood in the proppant filled packed bed saturated with MLP Crude Oil

## Secondary brine flood

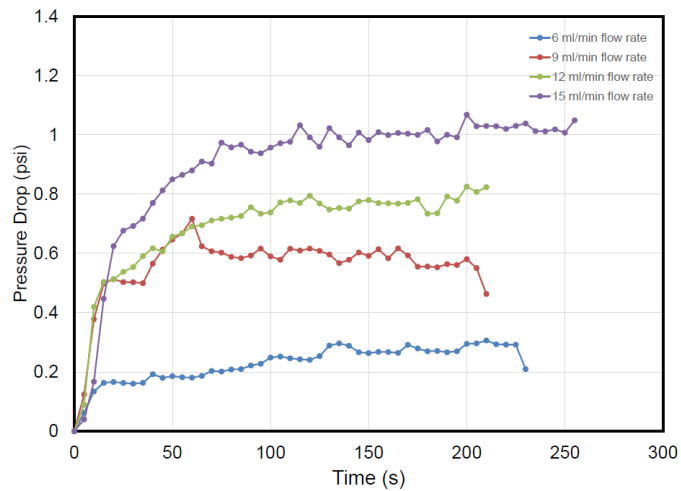


**Figure S11.** Secondary brine flood in the proppant filled packed bed

Also, no significant change in pack permeability was observed when the permeability of pack during primary and secondary brine flood were compared in this case. The results are summarized in Table S7.

**Table S7.** Summary of permeability calculations from sand pack analysis (primary and secondary brine flood)

Stage	Slope	KA/ $\mu$ L	$\mu$ (cP)	A (cm <sup>2</sup> )	L (cm)	K (D)	K(mD)
Primary Flood	3.07	3.07	1.02	0.55	25.93	147.30	147302
Secondary Flood	3.05	3.05	1.02	0.55	25.93	146.24	146237.2

The saturation of oil in the pack after oil and foam flood is measured and presented in table S8.

**Table S8.** Summary of calculations related to oil saturation in the sand pack after oil and foam flood in 66.7 kppm high salinity brine systems

System	Pore Volume (mL)	Volume of Flooded Oil (mL)	Volume of Collected Oil (mL)	Oil Saturation after Oil Flood (%)	Volume of Flooded Foam (liquid) (mL)	Volume of Collected Oil (mL)	Oil Saturation after Foam Flood (%)
Surf 1wt% 66.7kppm	7.69	76.34	59.8	97.96	11.37	18.2	30.17
PECNP:Surf 4:6 66.7 kppm	7.58	75.01	59.6	84.47	11.36	18.1	17.02

### **Raman Spectroscopy:**

#### **632.8 nm excitation wavelength post processing with Matlab:**

The mixture of PECNP and surfactant was fit with the model basis spectra (consisting of average spectra of PECNP and surfactant) using the least-squares method described by Shafer-Peltier using MATLAB [6]. Pre-processing of the spectra included fitting with a fifth degree of polynomial using MATLAB's polyfit function. Vectors representing each fit were created using the polyval function and residuals of each fit were determined. An average of three to four spectra were then used (except in the case of the PECNP:Surf complex spectra) for further analysis.

Cosmic rays were removed manually and Matlab's smoothing function was used to bin neighboring points to remove digital noise. The magnified region of interest was selected and normalized to initial data points at  $1000\text{ cm}^{-1}$  (lowering the curves with the magnitude of intensity at  $1000\text{ cm}^{-1}$ ). Figure S12 represents the normalized bands in magnified region  $1000\text{-}1025\text{ cm}^{-1}$  for surfactant and PECNP in 33.3 kppm brine, clearly illustrating the intensifying the  $1014\text{ cm}^{-1}$  band.

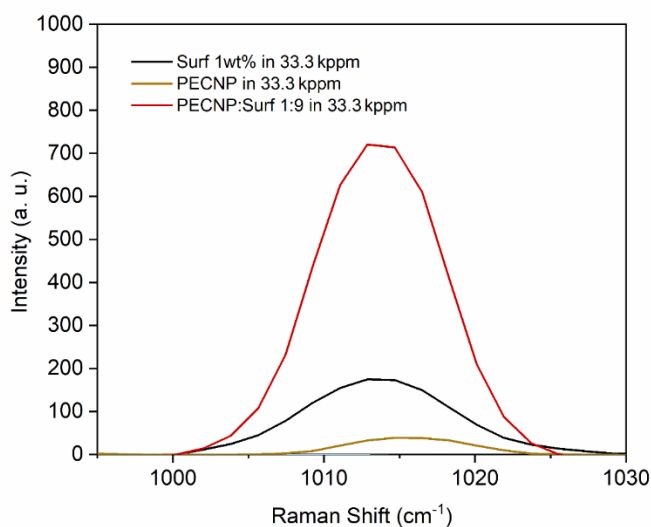


**Figure S12.** Normalized bands in magnified region  $1000\text{-}1025\text{ cm}^{-1}$  for surfactant and PECNP in 33.3 kppm brine

## **References**

- [1] Hosseini, H.; Tsau, J.; Barati, R. Lowering Fresh Water Usage in Hydraulic Fracturing by Stabilizing  $\text{scCO}_2$  Foam with Polyelectrolyte Complex Nanoparticles Prepared in High Salinity Produced Water. **2018**, *Society of Petroleum Engineers. SPE-189555-MS*.
- [2] Tewes, F.; Pierre, M.; Boury, F. Dynamical and Rheological Properties of Fluorinated Surfactant Films Adsorbed at the Pressurized  $\text{CO}_2\text{-H}_2\text{O}$  Interface. **2011**, *27*, 8144–52.
- [3] Boury, F.; Ivanova, T.; Panaieotov, I; Proust, J. E. Dilatational Properties of Adsorbed Poly(D,L-

- lactide) and Bovine Serum Albumin Monolayers at the Dichloromethane/Water Interface. *Langmuir*. **1995**, *11*, 1636–44.
- [4] Nazari, N.; Tsau, J; Barati, R. CO<sub>2</sub> Foam Stability Improvement Using Polyelectrolyte Complex Nanoparticles Prepared in Produced Water. *Energies*. **2017**, *10* (4), 516.
- [5] Anandan, R.; Johnson, S.; Barati, R. Polyelectrolyte Complex Stabilized CO<sub>2</sub> Foam Systems for Hydraulic Fracturing Application. *Society of Petroleum Engineers*. **2017**, *SPE-187489-MS*.
- [6] Shafer-Peltier, K. E.; Haka, A.S.; Fitzmaurice, M.; Crowe, J.; Myles. J.; Dasari, R. R. Raman microspectroscopic model of human breast tissue: Implications for breast cancer diagnosis in vivo. *J Raman Spectrosc*. **2002**, *33*, 552–563.